J|A|C|S ARTICLES

Published on Web 10/13/2009

Oligoyne Single Molecule Wires

Changsheng Wang,[†] Andrei S. Batsanov,[†] Martin R. Bryce,*[,†] Santiago Martín,[‡] Richard J. Nichols,*[,‡] Simon J. Higgins,[‡] Víctor M. García-Suárez,[§] and Colin J. Lambert*[,§]

Department of Chemistry and Centre for Molecular and Nanoscale Electronics, Durham University, Durham DH1 3LE, United Kingdom, Centre for Nanoscale Science and Department of Chemistry, University of Liverpool, Liverpool, L69 7ZD, United Kingdom, and Department of Physics, Lancaster University, Lancaster, LA1 4YB, United Kingdom

Received November 6, 2008; E-mail: m.r.bryce@durham.ac.uk; r.j.nichols@liverpool.ac.uk; c.lambert@lancaster.ac.uk

Abstract: We report the electrical conductance at the single molecule level of the oligoyne molecular wires Py-(C≡C)$_n$-Py (n = 1, 2 and 4; Py = 4-pyridyl) using STM-molecular break junction techniques in Au|molecule|Au configurations. The conductance histograms reveal multiple series of peaks attributed to differing contact geometries between the pyridyl head groups and the gold electrodes. Both experimental and theoretical evidence point to the higher conduction groups being related to adsorption of the pyridyl group at more highly coordinated sites such as step edges or alongside gold adatoms. All three conduction groups in the oligoyne series show a remarkably low β value of (0.06 ± 0.03) Å^{-1}, that is, the conductance is almost independent of molecular length. 4,4′-Bipyridyl studied under the same conditions does not follow this exponential decay series. Theoretical calculations using a combination of density functional theory and nonequilibrium Green's function formalism support the experimental results. We conclude that oligoynes and polyynes are a very promising class of molecular wires for integration into electronic circuitry.

Introduction

There is great interest in measuring and controlling electrical current through single molecules that are wired to two electrodes. Experimental studies, combined with theoretical calculations, provide insights into the mechanisms of charge transport in tailored nanoscale junctions and probe the interplay of molecular structure, electronic structure and single molecule conductance. These studies are crucial in the development of molecular electronic devices and related technologies including sensors based on the electrical detection of individual molecular binding events.[1] A growing number of experimental techniques are now being used for the measurements of charge transport through either single molecules or small ensembles of molecules. These include mechanically formed break junctions,[2−7] or break junctions formed by scanning probe microscopy techniques based on either STM[8−12] or conducting AFM.[13,14] It is clear that the measured conductance values depend not only on the molecule(s) in the junction but also on other important parameters, namely, the electrodes, the detailed contact geometry (i.e., hybridization at the molecule-electrode interfaces),[15−18] the temperature[19,20] and the local environment of the system

[†] Department of Chemistry, Durham University.
[‡] Department of Chemistry, University of Liverpool.
[§] Department of Physics, Lancaster University.

(1) Reviews: (a) Tour, J. M. *Acc. Chem. Res.* **2000**, *33*, 791–804. (b) Carroll, R. L.; Gorman, C. B. *Angew. Chem., Int. Ed.* **2002**, *41*, 4378–4400. (c) Maruccio, G. R.; Cingolani, R.; Rinaldi, R. *J. Mater. Chem* **2004**, *14*, 4378542–554. (d) Troisi, A.; Ratner, M. A. *Small* **2006**, *2*, 172–181. (e) James, D. K.; Tour, J. M. *Aldrichim. Acta* **2006**, *39* (2), 47–56. (f) Weibel, N.; Grunder, S.; Mayor, M. *Org. Biomol. Chem.* **2007**, *5*, 2343–2353. (g) Chen, F.; Hihath, J.; Huang, Z.; Li, X.; Tao, N. J. *Annu. Rev. Phys. Chem.* **2007**, *58*, 535–564. (h) Akkerman, H. B.; de Boer, B. *J. Phys.: Condens. Matter* **2008**, *20*, 013001.
(2) Reed, M. A.; Zhou, C.; Muller, C. J.; Burgin, T. P.; Tour, J. M. *Science* **1997**, *278*, 252–254.
(3) Kergueris, C.; Bourgoin, J. P.; Palacin, S.; Esteve, D.; Urbina, C.; Magoga, M.; Joachim, C. *Phys. Rev. B* **1999**, *59*, 12505–12513.
(4) Weber, H. B.; Reichert, J.; Ochs, R.; Beckmann, D.; Mayor, M.; von Lohneysen, H. *Phys. E* **2003**, *18*, 231–232.
(5) Reichert, J.; Ochs, R.; Beckmann, D.; Weber, H. B.; Mayor, M.; von Lohneysen, H. *Phys. Rev. Lett.* **2002**, *88*, 176804.
(6) Park, H.; Lim, A. K. L.; Alivisatos, A. P.; Park, J.; McEuen, P. L. *Appl. Phys. Lett.* **1999**, *75*, 301–303.
(7) Grüter, L.; González, M. T.; Huber, R.; Calame, M.; Schönenberger, C. *Small* **2005**, *1*, 1067–1070.
(8) Yazdani, A.; Eigler, D. M.; Lang, N. D. *Science* **1996**, *272*, 1921–1924.
(9) Xu, B. Q.; Tao, N. J. *Science* **2003**, *301*, 1221–1223.
(10) Dorogi, M.; Gomez, J.; Osifchin, R.; Andres, R. P.; Reifenberger, R. *Phys. Rev. B* **1995**, *52*, 9071–9077.
(11) Haiss, W.; van Zalinge, H.; Higgins, S. J.; Bethell, D.; Höbenreich, H.; Schiffrin, D. J.; Nichols, R. J. *J. Am. Chem. Soc.* **2003**, *125*, 15294–15295.
(12) Haiss, W.; Nichols, R. J.; van Zalinge, H.; Higgins, S. J.; Bethell, D.; Schiffrin, D. J. *Phys. Chem. Chem. Phys.* **2004**, *6*, 4330–4337.
(13) Cui, X. D.; Primak, A.; Zarate, X.; Tomfohr, J.; Sankey, O. F.; Moore, A. L.; Moore, T. A.; Gust, D.; Harris, G.; Lindsay, S. M. *Science* **2001**, *294*, 571–574.
(14) Leatherman, G.; Durantini, E. N.; Gust, D.; Moore, T. A.; Moore, A. L.; Stone, S.; Zhou, Z.; Rez, P.; Liu, Y. Z.; Lindsay, S. M. *J. Phys. Chem. B* **1999**, *103*, 4006–4010.
(15) McCreery, R. L.; Viswanathan, U.; Kalakodium, R. P.; Nowak, A. M. *Faraday Discuss.* **2006**, *131*, 33–43.
(16) Lindsay, S. M.; Ratner, M. A. *Adv. Mater.* **2007**, *19*, 23–31.
(17) Hu, Y.; Zhu, Y.; Gao, H.; Gao, H. *Phys. Rev. Lett.* **2005**, *95*, 156803.
(18) Li, C.; Pobelov, I.; Wandlowski, T.; Bagrets, A.; Arnold, A.; Evers, F. *J. Am. Chem. Soc.* **2008**, *130*, 318–326.
(19) Haiss, W.; van Zalinge, H.; Bethell, D.; Ulstrup, J.; Schiffrin, D. J.; Nichols, R. J. *Faraday Discuss.* **2006**, *131*, 253–264.

(vacuum or air, solvent, etc.).[21,22] Key molecular features that influence the conductance are: the extent of conjugation,[23,24] the nature of the terminal anchor groups (e.g., thiol, amine, carboxylic acid),[25] the detailed conformation[26,27] and the tilt angle[28,29] of the molecule in the junction.

To enhance electronic communication over nanometer distances, conjugated molecules which possess delocalized π-systems and low HOMO−LUMO gaps are attractive targets. In this context, oligo(phenyleneethynylene), (OPE) [i.e., $(C_6H_4-C\equiv C-)_n$] and oligo(phenylenevinylene), (OPV) [i.e., $(C_6H_4-CH=CH-)_n$] derivatives end-capped with thiol units have been integrated into device structures and their single molecule conductance values obtained.[30,31] The higher conductance for OPV derivatives, compared to OPE, has been explained by the longer vinyl bond (C=C length ca. 1.35 Å) in OPV disrupting the conjugation of the backbone less than the shorter ethynyl linkage (C≡C length ca. 1.22 Å) in OPE, that is, there is less bond alternation and a smaller HOMO−LUMO gap in OPV compared to OPE.[24]

We identified polyynes[32] $[(C\equiv C-)_n]$ as a class of conjugated compounds that have not been explored experimentally in single molecule junctions. Polyynes comprise an array of *sp*-hybridized carbon atoms with approximately cylindrical electron delocalization along a one-dimensional, rigid-rod, length-persistent backbone.[33] They are, therefore, very appealing linear molecular wires where electron transport along the chain is independent of rotation around the polyyne single bonds—a feature which makes them clearly distinct from other conjugated oligomers, for example, OPVs and OPEs, where the barrier to rotation about single bonds in the backbone is low[34,35] and conjugation is interrupted when the phenyl rings are rotated with respect to each other. A previous experimental study of the optical properties of silyl end-capped oligoynes $[(C\equiv C-)_n]$ ($n = 2-10$) established that they possess extensive conjugation which was supported by theoretical models of the third-order nonlinear optical response as a function of the number of alkyne units.[36] Analogous data for ligated platinum end-capped systems ($n = 3-6$, 8, 10, 12) are also known.[37] An *ab initio* calculation of thiolate-capped oligoynes ($n = 2-8$) in contact with gold electrodes suggested almost perfect molecular wire behavior. The conductance was calculated to be an order of magnitude higher compared to other conjugated oligomers, weakly dependent on the applied bias and almost independent of the length of the oligoyne chain.[38] In a recent calculation of pyridyl end-capped molecules,[32] where the conductance is found to be lower, the weak length dependence persists and moreover a pronounced sigmoidal $I-V$ characteristic is predicted. We now report experimental studies on the pyridyl end-capped systems **1**−**3** and compare these with theory. As a benchmark, data are also presented for 4,4′-bipyridyl **4** (Figure 1).

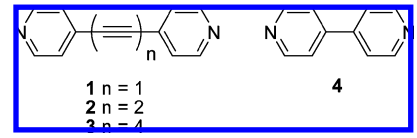

Figure 1. Molecular structures of the compounds used in this study.

Experimental and Theoretical Methods

Synthesis. Compounds **1**[39] and **2**[40] (Figure 1) were synthesized by the literature routes.

1,8-Di(4-pyridyl)-1,3,5,7-octatetrayne 3. (4-Pyridyl)-1,3-butadiyne[41] (0.191 g, 1.5 mmol), $PdCl_2(PPh_3)_2$ (21 mg, 2 mol %) and CuI (7 mg) were mixed in THF (20 mL). Triethylamine (3 mL) was added and oxygen was bubbled through the mixture at 20 °C for 2 h with stirring to obtain a pale brown solution. The addition of oxygen was stopped and the mixture was stirred for an additional 10 h until no unreacted butadiyne was present. The solution was evaporated to dryness. The brown solid residue was chromatographed on a silica column (eluent 1:1 v/v DCM-acetone) to afford a yellow solid, which was crystallized from ethyl acetate to yield greenish-yellow needles (59 mg, 31%), mp: the solid became dark brown at >160 °C; no clear mp was observed on heating up to 350 °C; ^{1}H NMR ($CDCl_3$, 400 MHz) $\delta = 7.37$ (d, $J = 6.2$ Hz, 4H), 8.63 (d, $J = 6.2$ Hz, 4H); ^{13}C NMR ($CDCl_3$, 100.6 MHz) $\delta =$ 63.6, 68.4, 74.8, 78.0, 126.4, 128.6, 150.0. Anal. Calcd for $C_{18}H_8N_2$: C, 85.70; H, 3.20; N, 11.10. Found: C, 85.64; H, 3.26; N, 11.22. A single crystal (yellow needle) was obtained by slow evaporation of a chloroform solution of the compound. The molecular structure of compound **3**, obtained from an X-ray crystal structure analysis, is described in the Supporting Information.

Conductance Measurements. Both the $I(s)$ and the in situ break junction (BJ) techniques use an STM for single molecule conductance determination, but they differ in how the junction is formed. In the $I(s)$ technique (I = current and s = distance) a gold STM tip is brought to a fixed distance above the gold surface covered with

(20) Jones, D. R.; Troisi, A. *J. Phys. Chem. C* **2007**, *111*, 14567–14573.
(21) Long, D. P.; Lazorcik, J. L.; Mantooth, B. A.; Moore, M. H.; Ratner, M. A.; Troisi, A.; Tour, J. M.; Shashidhar, R. *Nat. Mater.* **2006**, *5*, 901–908.
(22) (a) Cao, H.; Jiang, J.; Ma, J.; Luo, Y. *J. Am. Chem. Soc.* **2008**, *130*, 6674–6675. (b) Leary, E.; Hobenreich, H.; Higgins, S. J.; van Zalinge, H.; Haiss, W.; Nichols, R. J.; Finch, C. M.; Grace, I.; Lambert, C. J.; McGrath, R.; Smerdon, J. *Phys. Rev. Lett.* **2009**, *102*, 086801.
(23) Salomon, A.; Cahen, D.; Lindsay, S.; Tomfohr, J.; Engelkes, V. B.; Frisbie, C. D. *Adv. Mater.* **2003**, *15*, 1881–1890.
(24) Kushmerick, J. G.; Holt, D. B.; Pollack, S. K.; Ratner, M. A.; Yang, J. C.; Schull, T. L.; Naciri, J.; Moore, M. H.; Shashidhar, R. *J. Am. Chem. Soc.* **2002**, *124*, 1065410655. It should be noted that in this communication the OPE and OPV derivatives studied experimentally have different end groups. The OPE has terminal -C_6H_4-S units, whereas the OPV has terminal -C_6H_4-CH_2-S units.
(25) Chen, F.; Li, X.; Hihath, J.; Huang, Z.; Tao, N. *J. Am. Chem. Soc.* **2006**, *128*, 2135–2141.
(26) Venkataraman, L.; Klare, J. E.; Nuckolls, C.; Hybertsen, M. S.; Steigerwald, M. L. *Nature* **2006**, *442*, 904–907.
(27) Pauly, F.; Viljas, J. K.; Cuevas, J. C.; Schön, G. *Phys. Rev. B* **2008**, *77*, 155312.
(28) Haiss, W.; Wang, C.; Grace, I.; Batsanov, A. S.; Schiffrin, D. J.; Higgins, S. J.; Bryce, M. R.; Lambert, C. J.; Nichols, R. J. *Nat. Mater.* **2006**, *5*, 995–1002.
(29) Haiss, W.; Wang, C.; Jitchati, R.; Grace, I.; Martín, S.; Batsanov, A. S.; Higgins, S. J.; Bryce, M. R.; Lambert, C. J.; Jensen, P. S.; Nichols, R. J. *J. Phys.: Condens. Matter* **2008**, *20*, 374119.
(30) Seferos, D. W.; Trammell, S. A.; Bazan, G. C.; Kushmerick, J. G. *Proc. Natl. Acad. Sci. U.S.A.* **2005**, *102*, 8821–8825.
(31) Huber, R.; González, M. T.; Wu, S.; Langer, M.; Grunder, S.; Horhoiu, V.; Mayor, M.; Bryce, M. R.; Wang, C.; Jitchati, R.; Schönenberger, C.; Calame, M. *J. Am. Chem. Soc.* **2008**, *130*, 1080–1084.
(32) Garcia-Suarez, V. M.; Lambert, C. J. *Nanotechnology* **2008**, *19*, 455203.
(33) (a) Szafert, S.; Gladysz, J. A. *Chem. Rev.* **2003**, *103*, 4175–4205. (b) Szafert, S.; Gladysz, J. A. *Chem. Rev.* **2006**, *106*, PR1–PR33.
(34) Taylor, J.; Brandbyge, M.; Stokbro, K. *Phys. Rev. B* **2003**, *68*, 121101.
(35) James, P. V.; Sudeep, P. K.; Suresh, C. H.; Thomas, K. G. *J. Phys. Chem. A* **2006**, *110*, 4329–4337.
(36) Slepkov, A. D.; Hegmann, F. A.; Eisler, S.; Elliott, E.; Tykwinski, R. R. *J. Chem. Phys.* **2004**, *120*, 6807–6810.
(37) Samoc, M.; Dalton, G. T.; Gladysz, J. A.; Zheng, Q.; Velkov, Y.; Ågren, H.; Norman, P.; Humphrey, M. G. *Inorg. Chem.* **2008**, *47*, 9946–9957.
(38) Crljen, Ž.; Baranoviæ, G. *Phys. Rev. Lett.* **2007**, *98*, 116801.
(39) Champness, N. R.; Khlobystov, A. N.; Majuga, A. G.; Schröder, M.; Zyk, N. V. *Tetrahedron Lett.* **1999**, *40*, 5413–5416.
(40) Lee, C. K. Y.; Groneman, J. L.; Turner, P.; Rendina, L. M.; Harding, M. M. *Tetrahedron* **2006**, *62*, 4870–4878.
(41) West, K.; Wang, C.; Batsanov, A. S.; Bryce, M. R. *J. Org. Chem.* **2006**, *71*, 8541–8544.

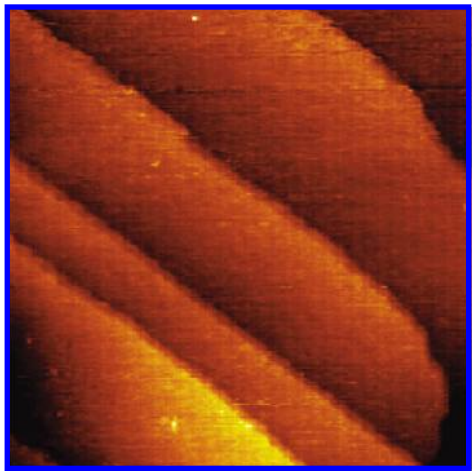

Figure 2. STM image of the Au(111) surface showing extended atomically flat terraces separated by monatomic steps; image size 150 nm × 150 nm.

the analyte molecule.[11,12] The current is then recorded as the STM tip is retracted from a surface until the molecule bridge(s) break, resulting in a current plateau followed by a step. In this way contact between the gold STM tip and the surface is avoided, with single molecular bridges then being formed between the gold substrate surface and gold STM tip. Current-distance [$I(s)$] curves are then analyzed statistically in the form of histogram plots to determine the single molecule conductance. These histograms are built by adding all the current (or conductance) points from ~100 current versus distance curves showing discernible plateaus which are taken as a characteristic of molecular bridge formation. In any given experimental run typically more than 1000 $I(s)$ scans were recorded, with exponential decay curves characteristic of tunnelling in the absence of molecular bridge formation and other indistinct curves being rejected from histogram analysis. For calculating errors all values encompassing a given histogram peak were statistically analyzed (using Origin) and the error is quoted as one standard deviation from the statistical spread of the points forming the histogram peak.

In contrast to the $I(s)$ method, the in situ break junction technique relies on the cleavage of metal break junctions formed between the STM tip and the metal surface. The break junction is formed by driving the tip a certain distance into the metal substrate.[9] The tip is then retracted until the metal contact cleaves and molecular bridges form within the break junction. These bridges then break upon further retraction of the tip and molecular conductance can be determined through statistical analysis of the current versus distance retraction curves.

Gold on glass slides (Arrandee, Schroeer, Germany) were flame-annealed with a Bunsen burner immediately prior to use. During this process the gold slide took on a slight orange hue and it was kept in this state for around 30 s by removing and reintroducing the sample into the flame to avoid overheating. This procedure is known to result in atomically flat Au(111) terraces.[42] Figure 2 shows an STM image of a flame annealed gold on glass sample. This shows a step and terrace structure with terraces up to about 50 nm wide. Oligoyne samples or bipyridyl were then adsorbed by immersion of their solutions in toluene (0.5 mM) for about 20 s. The relatively short immersion times and low concentrations are aimed at promoting low coverage on the gold slide which in turn favors single molecule events. After adsorption, the sample was washed in ethanol and then blown dry in a stream of nitrogen.

It has been previously shown for alkanedithiol molecule bridges between gold contact gaps that there is no unique value for the single molecule conductance, with multiple single molecule conductance values being evident.[12,18,43,44] In the case of alkanedithiols, three groups of peaks have been observed which have been attributed to differing contact morphologies between sulfur head groups and gold contacts or to different conductances for gauche and anti conformations.[12,18,43−45] Different contact configurations could arise from different adsorption sites of the sulfur with it positioned on top of a gold atom, at the midpoint between two gold atoms and in a hollow site at the center of a triangle of gold atoms, or could arise from the adsorption of contacting S atoms at either "flat" (terrace) or step sites. A recent study by Haiss et al.[45] supports the latter idea, which revealed that the higher conductance groups showed greater precedence on stepped or rough surfaces step sites, whereas the low conductance group were more evident on flat surface regions. The three sets of conductance values (labeled either L, M and H or A, B and C in order of increasing conductance) span over an order of magnitude in the case of octanedithiol.[12,18,43−45] In general, the lower conductance groups are more easily observed in the $I(s)$ technique, while the higher ones are more readily apparent in the in situ BJ technique, consistent with the notion that increased surface roughness promotes formation of higher conductance junctions.[45] With this in mind, we have used both the $I(s)$ and BJ techniques for each molecule to analyze differing conduction groups. Three sets of conductance values spanning 2 orders of magnitude have also been observed for a conjugated OPE derivative with thiol anchor groups and ascribed to different contact geometries.[46]

Theoretical Methods. The electronic and transport properties of pyridyl-capped oligoynes between gold leads were calculated with the SMEAGOL code.[47] SMEAGOL uses the Hamiltonian provided by the density functional theory[48] code SIESTA[49] to obtain self-consistently the density matrix, the electron transmission coefficients and the current within the nonequilibrium Green's function (NEGF) formalism.[50] The calculations used a double-ζ polarized basis set to span the valence orbitals, which is sufficient to achieve basis set convergence. An energy cutoff of 200 Ry was used to define the real-space grid and the local density approximation[51] was employed to calculate the exchange and correlation energy, which works relatively well in noble metals and light elements. The molecular coordinates were relaxed until all forces were <0.05 eV /Å. The gold leads were grown along the (111) direction and 9 atoms per layer were used. The system was made periodic along the directions perpendicular to the transport direction (z) and only the gamma point was employed, which was sufficient to converge the transmission coefficients. We had to use 5 layers of gold on each electrode to converge the system along the transport direction. The number of atoms involved explicitly in the calculations ranged from 104 for $n = 1$ to 110 for $n = 4$. A corrected position of the Fermi energy relative to the LUMO is obtained by shifting the position of the LUMO orbital with a self-energy correction. This takes into account the electron affinity calculated

(42) Haiss, W.; Lackey, D.; Sass, J. K.; Besocke, K. H. *J. Chem. Phys.* **1991**, *95*, 2193–2196.
(43) Li, X.; He, J.; Hihath, J.; Xu, B.; Lindsay, S. M.; Tao, N. J. *J. Am. Chem. Soc.* **2006**, *128*, 2135–2141.
(44) Fujihira, M.; Suzuki, M.; Fujii, S.; Nishikawa, A. *Phys. Chem. Chem. Phys.* **2006**, *8*, 3876–3884.
(45) Haiss, W.; Martín, S.; Leary, E.; van Zalinge, H.; Higgins, S. J.; Bouffier, L.; Nichols, R. J. *J. Phys. Chem. C* **2009**, *113*, 5823–5833.
(46) Weibel, N.; Blaszczyk, A.; von Hanisch, C.; Mayor, M.; Pobelov, I.; Wandlowski, T.; Chen, F.; Tao, N. *Eur. J. Org. Chem.* **2008**, *13*, 6–149.
(47) Rocha, A. R.; García-Suárez, V. M.; Bailey, S.; Lambert, C.; Ferrer, J.; Sanvito, S. *Phys. Rev. B* **2006**, *73*, 085414.
(48) (a) Hohenberg, H.; Kohn, W. *Phys. Rev.* **1964**, *136*, B864–B871. (b) Kohn, W.; Sham, L. J. *Phys. Rev.* **1965**, *140*, A1133–A1138.
(49) Soler, J. M.; Artacho, E.; Gale, J. D.; García, A.; Junquera, J.; Ordejón, P.; Sanchez-Portal, D. *J. Phys.: Condens. Matter* **2002**, *14*, 2745–2779.
(50) (a) Keldysh, L. V. *Sov. Phys. JETP* **1965**, *20*, 1018–1022. (b) Caroli, C.; Combescot, R.; Nozieres, P.; Saint-James, D. *J. Phys. C* **1972**, *5*, 21–42.
(51) Perdew, J. P.; Zunger, A. *Phys. Rev. B* **1981**, *23*, 5048–5079.

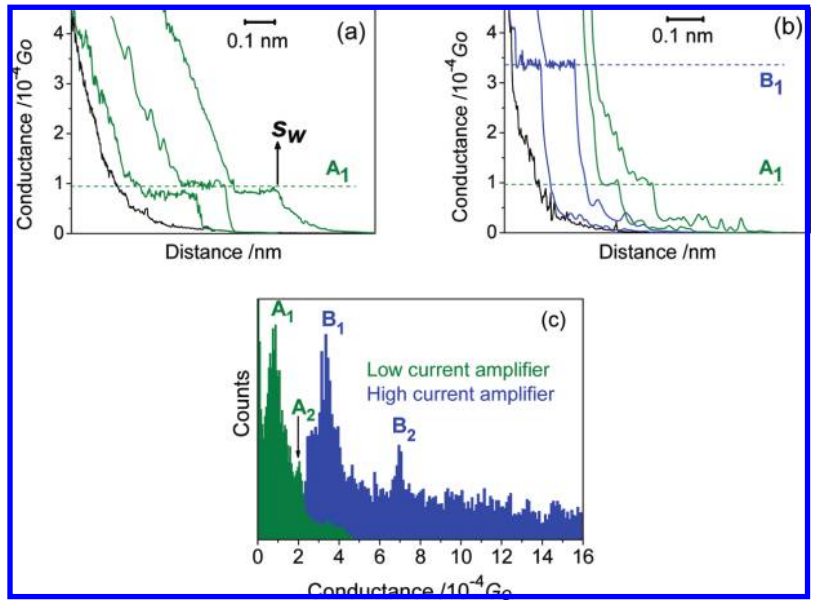

Figure 3. (a−b) Typical conductance traces of compound **1** ($n = 1$) using the $I(s)$ method at low set-point current (10−20 nA), using a low current amplifier, and high set-point current (60−80 nA), using a high current amplifier, respectively. The curves are shifted horizontally for clarity. (c) Conductance histograms built by adding together all the points of 85 and 105 conductance traces, respectively, that showed discernible plateaus such as those displayed in (a−b). Conductance data are presented in units of the conductance quantum $G_0 = 2e^2/h = 77.5\ \mu$S. $U_{tip} = 0.6$ V.

from differences between total energies of the neutral molecule and its singly charged anion radical. An additional shift is also applied in the opposite direction, which accounts for screening effects.[52−54] To calculate the latter we followed the procedure described by Quek et al.[55] (For more details, see the Supporting Information.)

Results and Discussion

Diaryloligo(poly)ynes are accessible via a range of synthetic methods and their stability decreases significantly with increasing chain length.[56−58] We chose pyridyl end-groups for our series of oligoynes **1**−**3** as previous work[9] had shown that the nitrogen atoms of 4,4′-bipyridyl **4** were suitable anchor points for single molecule measurements at electrode surfaces.[59]

Two techniques have been used in this study to determine the single molecule conductance, namely the $I(s)$ technique developed by Haiss et al.[11,12] and the in situ break junction technique developed by Xu and Tao.[9] (See the Experimental Section for further details.) Figure 3a shows typical conductance curves of compound **1** recorded using the $I(s)$ method at set-point currents of between 10−20 nA using a low current (high sensitivity) preamplifier in the STM scanner and at $U_{tip} = 0.6$ V. These retraction curves have been staggered along the x-axis to aid presentation. Retraction curves start at a set-point distance (s_0), from which the tip is withdrawn after temporarily switching off the feedback loop. Δs is the distance displacement from the set-point distance (s_0), the initial set-point distance of the tip from the surface at the start of an $I(s)$ scan. The plateaus seen in the traces are assigned to molecular bridge formation. The end of the plateau is marked by a rapid drop in conductance as the molecular junction cleaves either at the Au−adsorbate bond or Au−Au metallic bonds in the contacts.[43] The distance at which this occurs is defined as s_w, as marked in Figure 3a. The conductance plateau value is marked A_1 in Figure 3a. Figure 3b shows conductance traces recorded in a similar fashion albeit with higher set-point current values (60−80 nA) and at $U_{tip} = 0.6$ V, using a high current preamplifier. These higher set-point (I_0) values correspond to closer initial approach (s_0) of the tip to surface before retraction of the tip in the $I(s)$ scan. Under these conditions two pairs of peaks are observed, marked A and B in Figure 3b. Values for conductance plateaus from a large number of curves with both low and high current amplifier are collected in a conductance-histogram plot in Figure 3c where second values (A_2 and B_2) are just apparent.

Figure 4 shows data recorded using the STM-BJ method at $U_{tip} = 0.6$ V. This method involves the cleavage of metal−metal "break" junctions and it is expected that many more irregular junctions result than for the $I(s)$ method, because the latter avoids direct contact of the metal STM tip and surface and measurements are conducted on flat substrate areas. Nevertheless, similar current jump values, corresponding to A and B groups, are seen in retraction curves presented in Figure 4a. A corresponding histogram is seen in Figure 4b, which demonstrates close similarity between the A and B groups of peaks seen both in the $I(s)$ and BJ methods. A further set of higher conductance peaks (labeled C) is seen when a higher current STM current amplifier is used together with lower bias voltage, at $U_{tip} = 0.1$ V (Figure 4c and d); although this lower sensitivity amplifier does not allow for the observation of the low conductance

(52) Neaton, J. B.; Hybertsen, M. S.; Louie, S. G. *Phys. Rev. Lett.* **2006**, *97*, 216405–216408.
(53) Quek, S. Y.; Venkataraman, L.; Choi, H. J.; Louie, S. G.; Hybertsen, M. S.; Neaton, J. B. *Nano Lett.* **2007**, *7*, 3477–3482.
(54) Mowbray, D. J.; Jones, G.; Thygesen, K. S. *J. Chem. Phys.* **2008**, *128*, 111103–111107.
(55) Quek, S. Y.; Kamenetska, M.; Steigerwald, M. L.; Choi, H. J.; Louie, S. G.; Hybertsen, M. S.; Neaton, J. B.; Venkataraman, L. *Nat. Nanotechnol.* **2009**, *4*, 230–234.
(56) Luu, T.; Elliott, E.; Slepkov, A. D.; Eisler, S.; McDonald, R.; Hegmann, F. A.; Tykwinski, R. R. *Org. Lett.* **2005**, *7*, 51–54.
(57) Simpkins, S. M. E.; Weller, M. D.; Cox, L. R. *Chem. Commun.* **2007**, 4035–4037.
(58) Kendall, J.; McDonald, R.; Ferguson, M. J.; Tykwinski, R. R. *Org. Lett.* **2008**, *10*, 2163–2166.
(59) During the course of our work single molecule studies were reported on (a) 1,2-di(pyridin-4-yl)ethene and 1,2-di(pyridin-4-yl)ethane: Zhou, X.-S.; Chen, Z.-B.; Liu, S.-H.; Jin, S.; Liu, L.; Zhang, H.-M.; Xie, Z.-X.; Jiang, Y.-B.; Mao, B.-W. *J. Phys. Chem. C* **2008**, *112*, 3935–3940. (b) 4,4′-bipyridine: see ref 55.

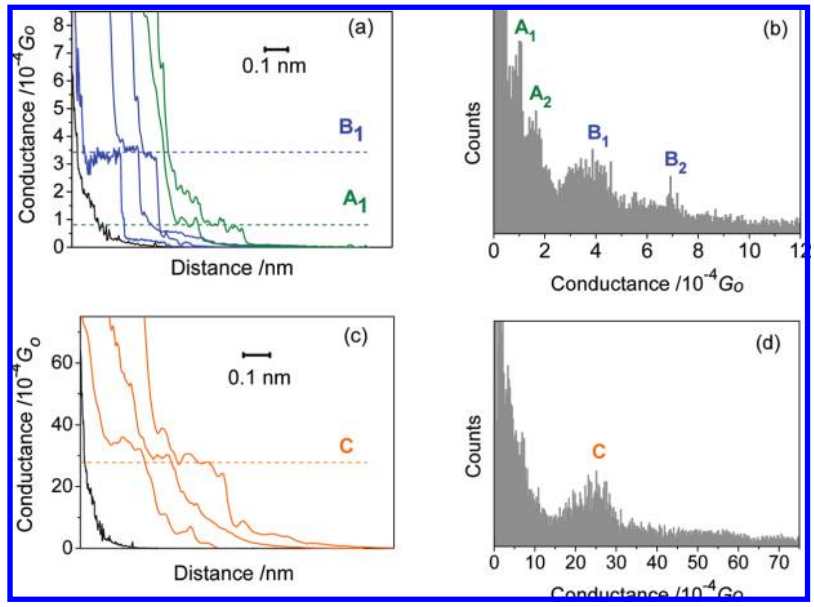

Figure 4. Typical conductance traces of compound **1** ($n = 1$) using (a) the STM-BJ method and (c) a higher current STM current amplifier together with lower bias voltage (0.1 V) to observe the highest conductance peak (labeled C). The curves in (a) and (c) are shifted horizontally for clarity. (b−d) Conductance histograms built by adding together all the points of 95 and 75 conductance traces, respectively, that showed discernible plateaus.

Table 1. Single Molecule Conductance Data for These Compounds, with Data for the A ("Low"), B ("Medium") and C ("High") Conductance Groups Tabulated

	conductance /10^{-4} G_0		
compound	A	B	C
1 ($n = 1$)	0.90 ± 0.30	3.45 ± 0.43	28.9 ± 5.20
2 ($n = 2$)	0.62 ± 0.13	2.93 ± 0.37	24.9 ± 3.06
3 ($n = 4$)	0.51 ± 0.11	2.41 ± 0.33	21.6 ± 3.05
4 ($n = 0$)	1.34 ± 0.17	5.38 ± 0.64	75.5 ± 15.3

groups. The occurrence of these different conductance groups could be ascribed to different contact geometries as discussed above, i.e. with the nitrogen−gold contacts occupying different surface coordination sites. These could be top, bridge or hollow sites on terraces or more highly coordinated step-edge sites, as discussed later in the text. The respective data of the single molecule conductances for compounds **1**−**4** are summarized in Table 1.

4,4-Bipyridine **4** is the control compound which has been studied previously. Our values (Table 1 and Figure 6) are 1.34 ± 0.17, 5.38 ± 0.64 and $75.5 \pm 15.3 \times 10^{-4}$ G_0 for A, B and C groups, respectively. These data compare favorably with those for **4** reported by Quek et al.[55] (1.6×10^{-4} G_0 and 6.0×10^{-4} G_0 extending to ca. 3×10^{-3} G_0) and differ from the data reported by Xu and Tao[9] (1×10^{-2} G_0) and Zhou et al.[59] (0.59×10^{-3} and 4.79×10^{-3}).

As explained in the literature,[28,45,60] careful calibration of the tip-to-substrate distance allows an estimation of the gap separation at which the molecular junction is cleaved. This calibration is achieved by obtaining $\mathrm{d}\ln(I(s))/\mathrm{d}s$ in the distance range of interest and extrapolating to the point contact conductance to obtain the zero tip-to-substrate reference separation. The retraction distance measured in an $I(s)$ scan from the initial set-point distance (s_0) can then be recalibrated to the estimated separation between tip and sample. In a given $I(s)$ scan current steps occur

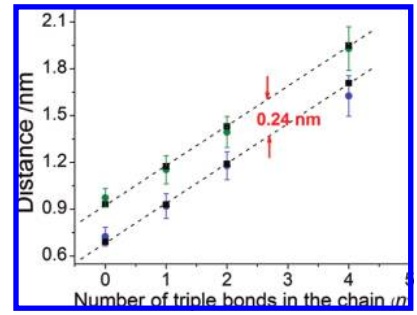

Figure 5. Experimentally determined average break-off distance ($s_{\text{break-off}} = s_w + s_0$) for group A (green, upper line) and group B (blue, lower line) events for compounds with $n = 0$, 1, 2, and 4 as measured with the $I(s)$ technique. The results of the molecular modeling calculation schematically depicted in Figure 9 are shown as black squares together with a linear fit.

at s_w (Figure 3); since the $I(s)$ scan starts at the separation of s_0 the experimentally measured break-off distances ($s_{\text{break-off}}$) is then given by ($s_0 + s_w$). This experimentally measured break-off distance can then be compared to the length of the molecule (for compound **3** obtained from the crystal structure and for the other compounds from standard bond lengths taking into account the rigidity of these systems). Such a comparison is shown in Figure 5 for both groups A and B. From this figure it can be seen that the $s_{break\text{-}off}$ values are close to distances obtained for each of the molecules extended between gold contacts, with the distance being that between the respective gold contact atoms at each end of the molecular wire.

The collected conductance values for groups A, B and C for compounds **1**−**3** (i.e., $n = 1$, 2 and 4) are plotted as logarithmic conductance versus n in Figure 6. All three conduction groups (A, B and C) show a similar length decay. The decay from $n = 1-4$ is very shallow with an apparent β value of (0.06 ± 0.03) Å^{-1}. For comparison the conductance for bipyridyl **4** ($n = 0$) is also shown. This does not lie on the exponential decay line, since the latter is associated with the oligoyne backbone. The very low attenuation factor of 0.06 Å^{-1} is comparable with observations for some other highly conjugated, low bandgap

(60) Sedghi, G.; Sawada, K.; Esdaile, J. L.; Hoffmann, M.; Anderson, H. L.; Bethell, D.; Haiss, W.; Higgins, S. J.; Nichols, R. J. *J. Am. Chem. Soc.* **2008**, *130*, 8582–8583.

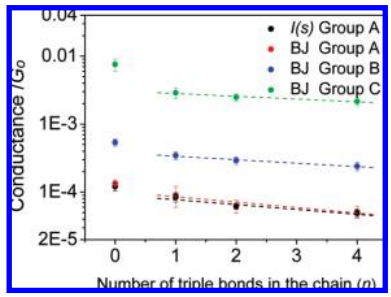

Figure 6. Logarithmic plot of single molecule conductance versus number of triple bonds in the chain (n) for groups A, B and C for compounds **1**−**4** (i.e., n = 1, 2, 4, 0, respectively). Data are shown for the $I(s)$ and STM break junction (BJ) techniques as marked.

systems. For instance, recent single molecule conductance measurements on a series of oligoporphyrins[60] gave $\beta = 0.04$ Å^{-1} and oligothiophenes[61] gave $\beta = 0.1$ Å^{-1}. It is noteworthy that a very similar β value (0.06 ± 0.005 Å^{-1}) to that found in the present work was obtained for a series of Zn-porphyrin-(C≡C)$_n$-C$_{60}$ dyads with oligoyne bridges (n = 1−4) in which photoinduced charge separation and charge recombination were studied as a function of D−A distance.[62] These complementary data from two very different techniques attest to the excellent transmission properties of oligoyne bridges. Electrochemical data on redox-active organometallic complexes in which two metal centers are bridged by oligoynes, and the evolution of intervalence charge transfer bands as a function of oligoyne length in mixed valence examples of such molecules, suggest that electronic communication between metal centers mediated by oligoynes does diminish,[63] albeit at much longer oligoyne lengths than those used in our study.

The shallow length decay observed experimentally is in qualitative agreement with the recent theoretical predictions[32] although there are significant differences, which we now investigate. The calculated conductance values for the longer molecules are particularly sensitive to the position of the Fermi energy. Values obtained using the Fermi energy E_F from the LDA-based SMEAGOL calculation show that conductance increases with molecular length, which is not in agreement with the experimental data. These discrepancies between LDA-based calculations and experimental observations are likely to originate from the use of mean field theories of DFT and the exclusion of many-electron interactions.[52−55] These many-body interactions are expected to shift resonances away from E_F and reduce the DFT-computed conductance. Within the current computational framework it is not possible to include these many-electron interactions. It is possible however to provide an estimate of the self-energy errors and to adjust accordingly the position of the LUMO (HOMO) with respect to E_F. The LUMO dominates transport since its position is much closer to E_F than the HOMO-related features (e.g., see Figure S5 in the Supporting Information). The position of the LUMO resonances for compounds **1**−**3** after correction for self-energy and screening are given in Table 2. By applying such corrections and fitting the LUMO to a Lorentzian form with the same width as in the

Table 2. Self-Energy Correction (Σ_{corr}), Final Position of the LUMO Resonance Relative to the Fermi Energy (E_{LUMO}) after Self Energy and Screening Corrections and Theoretical Values of the Conductance[a]

compound	Σ_{corr} (eV)	final E_{LUMO} relative to E_F (eV)	theoretical conductance/10^{-4} G_0	experimental conductance/ 10^{-4} G_0
1 (n = 1)	1.33	1.56	0.30	0.90 ± 0.30
2 (n = 2)	1.31	1.43	0.27	0.62 ± 0.13
3 (n = 4)	1.22	1.26	0.23	0.51 ± 0.11

[a] For comparison, the right-most column shows the experimental values for the A-series of conductance values from Table 1.

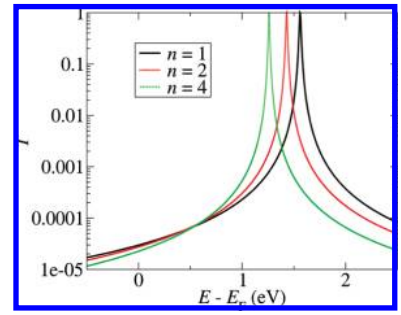

Figure 7. Self-energy corrected transmission curves for compounds **1** − **3** (n = 1, 2, 4).

ab initio calculations we obtain the curves shown in Figure 7[64] and the values for the zero-bias conductance stated in Table 2. These calculated conductances are much closer (within an order of magnitude) to the experimental values than those obtained without self-energy and screening corrections and yield a remarkably small β value of 0.034 Å^{-1}. Remaining discrepancies between the theoretical and experimental conductances could arise from states below the Fermi level and slight underestimation of the coupling strength; both these factors can increase the conductance.

We now turn to a possible origin for the differing conduction groups, A, B and C. As noted earlier in the text multiple conductance values have been recorded for alkanedithiols, where three groups of peaks have also been noted.[12,18,43−45] These different conductance groups have been attributed to differences in the coordination of the thiol headgroup with the gold surface, with the higher conductance groups being assigned to higher coordination sites which have been proposed to lead to higher electronic transmission.[45] To gain further insight into the differing conduction groups for the pyridyl end-capped oligoynes studied here we have analyzed average break-off distances for group A and B events. Figure 8 shows break-off distance histograms for compound **1** (n = 1), where $s_{break\text{-}off}$ has been calculated as described in the preceding text. Two histograms are shown on the same plot, the one peaking at shorter $s_{break\text{-}off}$ corresponds to the B events and the other at slightly longer $s_{break\text{-}off}$ corresponds to the A events. The measured difference between the two histogram peaks is 0.22 nm. Figure 5 shows that a similar phenomenon is seen for compounds **2**, **3** and **4** (n = 2, 4 and 0) with an average displacement of ca. 0.24 nm between

(61) Yamada, R.; Kumazawa, H.; Noutoshi, T.; Tanaka, S.; Tada, H. *Nano Lett.* **2008**, *8*, 1237–1240.
(62) Vail, S. A.; Krawczuk, P. J.; Guldi, D. M.; Palkar, A.; Echegoyen, L.; Tomé, J. P. C.; Fazio, M. A.; Schuster, D. I. *Chem.—Eur. J.* **2005**, *11*, 3375–3388.
(63) (a) Dembinski, R.; Bartik, T.; Bartik, B.; Monika Jaeger, M.; Gladysz, J. A. *J. Am. Chem. Soc.* **2000**, *122*, 810–822. (b) Le Stang, S.; Paul, F.; Lapinte, C. *Organometallics* **2000**, *19*, 1035–1043.
(64) The plot of the transmission coefficient $T(E)$ versus electron energy (E) presented in Figure 7 shows that electrons at the Fermi energy (E_F = 0) are controlled by the tail of $T(E)$. At room temperature, T_{room}, electrons within an energy range of ca. K_BT_{room} = 1/40 eV of E_F contribute to transport through this tail. The peak of $T(E)$ is >1 eV above E_F and, therefore, thermal activation "above the barrier" (i.e. via the LUMO) is negligible, because exp(1 eV/K_BT_{room}) ≈ exp(−40).

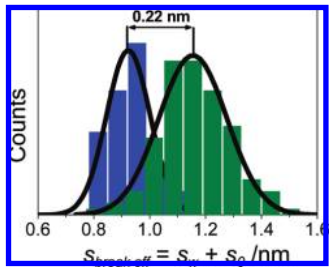

Figure 8. Histograms of break-off distances for compound **1** ($n = 1$). Two histograms are shown on the same plot, the one peaking at lower $s_{\text{break-off}}$ (blue) corresponds to the B events and the other at longer $s_{\text{break-off}}$ (green) corresponds to the A events. Histograms were generated through analysis of 120 break-off events.

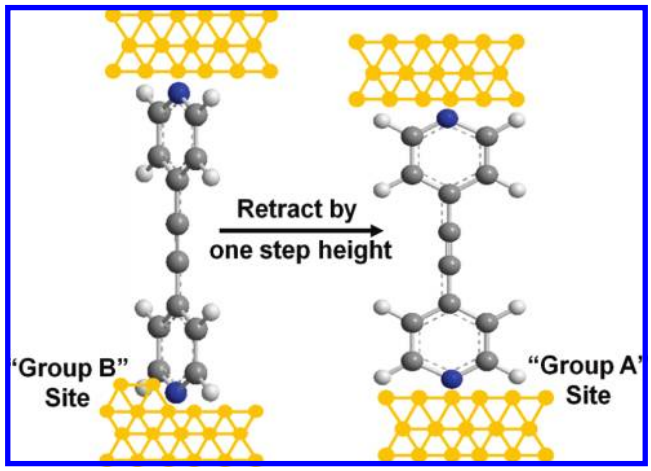

Figure 9. Cartoon for group "A" and "B" sites (see text); group A involves adsorption at a flat surface site while group B places the pyridyl group adsorbed at a step or similar high coordination site. As the junction is stretched in the STM retraction experiment, group B sites can be transformed into group A by pulling the pyridyl headgroup up by one gold step height (0.23 nm). See Figure 10 for a theoretical simulation using gold adatoms to model step edge adsorption.

group B and A events. The measured separation is close to a gold step height implying that the difference between group B and A is a structural transition involving a step edge. With this in mind we propose in Figure 9 a model for the difference. For group B a pyridyl headgroup is adsorbed at the base of a gold step edge or similar "lower lying" surface defect site; by pulling-up this headgroup by one gold step height this group B feature is transformed into a group A feature, accounting for the displacement measured from Figure 8.

In seeking a theoretical justification for the different experimentally observed conductance groups, we have considered within a computational framework the influence of surface coordination of the pyridyl contact group. Calculations show that for adsorption on flat Au(111) terraces, the most stable bonding geometry has the pyridine N atom positioned on top of a gold atom in preference to hollow or bridge sites (Figure S4 in the Supporting Information). The origin of the different conductance peaks can be modeled by placing gold adatoms on the surface next to the adsorbed pyridyl end groups. The largest change in the conductance occurs when the pyridyl rings are positioned alongside a gold adatom, so that it couples directly to the π system of the molecule (Figure 10 for compound **1**). This is in agreement with the calculations of Quek et al.[55] (and previous literature)[65] who found that the conductance of 4,4-bipyridine increased when the LUMO had a significant overlap

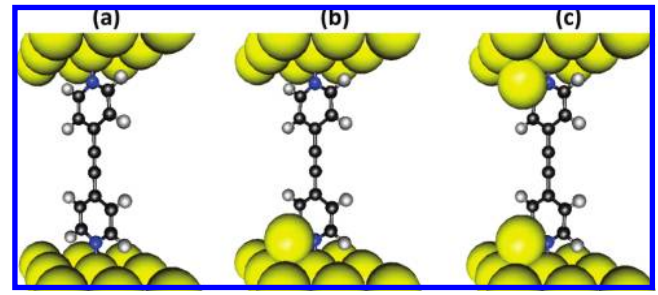

Figure 10. Illustration of compound **1** ($n = 1$) in different adsorption configurations between a pair of gold (111) contacts. (a) Compound **1** with both pyridyl nitrogen atoms adsorbed atop on a flat terrace, (b) one pyridyl group located alongside a gold surface adatom, (c) both pyridyl groups located alongside a gold adatom. Theoretically computed conductance increases from (a) to (c).

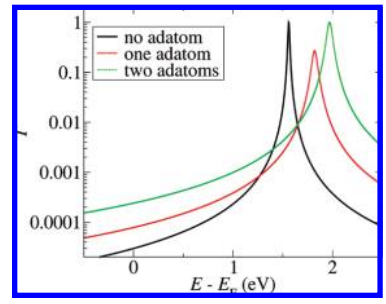

Figure 11. Self-energy corrected transmission curves for compound **1** calculated by including no gold adatoms (as in Figure 10a), one (Figure 10b) or two gold adatoms (one at each contact as in Figure 10c) on the surface coupled directly to the ring(s) of the molecule.

Table 3. Self-Energy Corrected Conductance Values Obtained for Molecule **1** with "Flat" Contacts (Figure 10a), One Gold Adatom on One Contact (Figure 10b) or One Gold Adatom on Each Contact (Figure 10c)

surface contact	conductance/10^{-4} G_0
No adatom	0.30
One gold adatom on one contact	0.78
One gold adatom on each contact	2.40

with adjacent gold atoms. When such atoms are included in the calculations the self-energy corrected curves shown in Figure 11 are obtained, showing a progressive increase in conductance for 0, 1, and 2 adatoms. The calculated conductance values are given in Table 3.

Conclusions

We have synthesized a series of oligoyne molecular wires end-capped with 4-pyridyl substituents [py-(C≡C)$_n$-py ($n = 1$, 2 and 4] and measured their electrical conductance at the single molecule level using STM-molecular break junction techniques in Au|molecule|Au configurations. Multiple series of peaks are observed in the conductance histograms which are ascribed to differing contact geometries between the pyridyl anchor groups and the gold electrodes. Experimental and theoretical evidence points to the higher conduction groups being related to adsorption of the pyridyl group at more highly coordinated sites such as step edges or alongside gold adatoms. A remarkable feature

(65) (a) Pérez-Jiménez, A. J. *J. Chem. Phys. B* **2005**, *109*, 10052–10060. (b) Stadler, R.; Thygesen, K. S.; Jacobsen, K. W. *Phys. Rev. B* **2005**, *72*, 241401(R). (c) Bagrets, A.; Arnold, A.; Evers, F. *J. Am. Chem. Soc.* **2008**, *130*, 9013–9018.

of the conductance data is the very low experimental and theoretical β values of (0.06 $\pm$ 0.03) Å^{-1} and 0.034 Å^{-1}, respectively. In other words, the conductance in the oligoyne series is only weakly dependent on molecular length, which is in marked contrast to OPV[66] and OPE systems.[67]

The oligoyne systems presented here are archetypical conjugated molecular wires formed from linear carbon chains with alternating single and triple bonds. The homologous series synthesized in this study gave rise to a well-defined electrical behavior in single molecule junctions with gold electrodes, showing a conductance almost independent of molecular length. For significantly longer systems than those studied here, it may be necessary to protect the molecules from chemical reaction or degradation, e.g. by molecular or supramolecular encapsulation strategies.[68] Overall, oligoyne systems are very promising candidates for molecular wires, which should be considered alongside other systems as building blocks in the construction of components for molecular electronics.

Acknowledgment. This work was supported by EPSRC under grants EP/C00678X/1 (Mechanisms of Single Molecule Conductance) and GR/S84064/01 (Controlled Electron Transport Through Single Molecules), QinetiQ and the British Department of Trade and Industry, Royal Society, Northwest Regional Development Agency, the EC FP7 ITN "FUNMOLS" project no. 212942 and the EC FP7 ITN "NANOCTM". S. M. acknowledges a postdoctoral fellowship from Ministerio de Educacion y Ciencia of Spain. We thank the NWGrid for computing resources.

Supporting Information Available: X-ray crystal structure of compound **3**; additional conductance data and details of the procedures used in the theoretical calculations; UV−vis absorption spectra of **1**, **2** and **3** in solution. This material is available free of charge via the Internet at http://pubs.acs.org.

JA9061129

(66) He, J.; Chen, F.; Li, J.; Sankey, O. F.; Terazono, Y.; Herrero, C.; Gust, D.; Moore, T. A.; Moore, A. L.; Lindsay, S. M. *J. Am. Chem. Soc.* **2005**, *127*, 90131384–1385.
(67) Liu, K.; Li, G.; Wang, X.; Wang, F. *J. Phys. Chem. C* **2008**, *112*, 4342–4349.
(68) Mohr, W.; Stahl, J.; Hampel, F.; Gladysz, J. A. *Chem.—Eur. J.* **2003**, *9*, 3324–3340.